Design of Orthogonal MIMO Handset antennas based on characteristic mode manipulation at frequency bands below 1 GHz

Li, Hui; Miers, Zachary; Lau, Buon Kiong

Published in:
IEEE Transactions on Antennas and Propagation

DOI:
10.1109/TAP.2014.2308530

2014

Document Version:
Peer reviewed version (aka post-print)

Design of Orthogonal MIMO Handset Antennas Based on Characteristic Mode Manipulation at Frequency Bands below 1 GHz

Hui Li, *Member, IEEE*, Zachary Miers, *Student Member, IEEE* and Buon Kiong Lau, *Senior Member, IEEE*

***Abstract*—Multi-antenna design in compact mobile handsets at frequency bands below 1 GHz is very challenging, since severe mutual coupling is commonly induced by simultaneous excitation of the chassis' fundamental dipole mode by more than one antenna element. To address this problem, a novel multi-antenna design approach is proposed herein to obtain efficient and uncorrelated antennas. By manipulating the chassis structure, more than one characteristic mode is enabled to resonate at frequencies below 1 GHz. With proper excitations for different characteristic modes, which are orthogonal to each other, well matched multi-antennas with low coupling and correlation are achieved. A chassis loaded with two T-shaped metal strips above its longer edges is taken as an example modification to illustrate the effectiveness of the proposed design approach at 900 MHz. This modification creates a new characteristic mode which resonates near 900 MHz. Afterward, two antenna feeds were designed to efficiently excite the chassis' fundamental dipole mode and the T-strip mode with very low correlation. The T-strip antenna covers LTE Band 8 (880-960 MHz), and the dipole mode antenna covers both LTE Band 5 (824-894 MHz) and LTE Band 8. The proposed dual-antenna design was found to outperform a reference design significantly, both with and without user interactions (i.e., one-hand and two-hand data grips). Practical aspects of mobile handset antennas are also investigated. The prototype was also fabricated and measured, and the measured results show reasonable agreements with the simulated results.**

***Index Terms*—MIMO systems, mutual coupling, antenna array, mobile antenna.**

I. Introduction

THE increasing popularity of smart phones and mobile internet is spurring the fast-growing demand for high speed mobile communications, which is in turn leading to the widespread adoption of multiple-input multiple-output (MIMO) technology in wireless communication standards. MIMO utilizes multiple antennas in both base stations and terminals to enable linear increase in channel capacity with the number of antennas, without sacrificing additional frequency spectrum and transmitted power [1]. In user terminals, limited by their relatively small sizes, integration of multiple antennas is challenging. Severe mutual coupling between closely spaced terminal antennas degrades the terminals' MIMO performances, such as correlation, diversity gain and capacity [2].

Accordingly, many effective decoupling techniques have been reported in the literature [2], such as the use of multiport matching networks [3], ground plane modification [4], [5], neutralization line [6], and parasitic scatterer [7]. More recently, highly isolated terminal antennas are achieved by exciting three different characteristic modes of a 120 mm × 60 mm mobile chassis at 2.5 GHz [8]. However, the required matching network is complicated in this multi-antenna system, resulting in limited total antenna efficiencies in practice. Besides, most of the aforementioned decoupling techniques are only demonstrated for terminal applications at frequency bands above 1.8 GHz.

For frequencies below 1 GHz, the existing decoupling techniques are no longer adequate to enable good MIMO antenna design, especially when taking both mutual coupling and antenna bandwidth into consideration [9-11]. In [12], a compact multi-band dual antenna system has been proposed for the LTE operation, with large bandwidth and good isolation achieved simultaneously. However, the envelope correlation coefficient (ECC) as calculated from the far field patterns was found to be relatively high (i.e., around 0.5) in the low band, which degrades the capacity performance. The reason for high correlation is that the mobile chassis is of the right dimensions to provide only one resonant characteristic mode, which is commonly excited and shared by more than one antenna element, making space, angle and polarization diversities difficult to achieve.

From perspective of chassis mode, to mitigate the chassis-induced coupling, existing strategies are aimed at allowing only one antenna to excite the chassis (to obtain good bandwidth and gain performance), whereas the other antenna(s) minimizes chassis excitation by either: (1) optimizing the antenna location [13], (2) using magnetic antenna types as motivated by the electric and magnetic field distributions of the chassis' fundamental dipole mode [14], or (3) localizing the chassis current to the immediate vicinity of the antenna element [15]. However, the bandwidth of the non-chassis-exciting antenna(s) is usually limited due to it being electrically small and not making use of the electrically larger chassis to radiate.

Chassis modifications, such as etching a slot [16], implementing a wavetrap [17], [18] or mounting a parasitic scatterer [7], have been investigated for different applications. However, these methods are not intended for low-frequency

Manuscript received August 08, 2013. This work was supported in part by VINNOVA under grant no. 2009-04047, and in part by Vetenskapsrådet under grant nos. 2010-468 and 2012-4859. This paper was presented in part at the 2013 IEEE International Symposium on Antennas and Propagation, Orlando, FL, USA, Jul 7-13, 2013.

H. Li, Z. Miers and B. K. Lau are with the Department of Electrical and Information Technology, Lund University, 221 00 Lund, Sweden (e-mail: Hui. Li, Zachary.Miers, Buon_Kiong.Lau@eit.lth.se).

multi-antenna designs from the perspective of characteristic mode modification. On the other hand, a current trend in mobile phone design is to use metallic structure(s) in the casing (e.g., bezels) for mechanical or aesthetics reasons, which also modify the chassis properties to some extent [19]. Unintentionally, due to the phenomenon of chassis excitation, the metallic structure often becomes a part of the antenna and varies the internal antenna performance. Sometimes, the metallic structure needs to be redesigned to restore the desired performance of the internal antennas [20]. In fact, Apple iPhone 4 even uses the metallic bezel in the housing of the phone as an external antenna [21].

In this context, we propose a novel approach to design multi-antennas in mobile handset by manipulating the chassis in a reasonable manner (or by opportunistic use of existing modifications), in order to allow more than one characteristic mode to be effectively excited below 1 GHz. As an example, a T-strip loaded chassis was studied. The T-strip addition to the chassis generates a new mode apart from the original fundamental dipole mode to resonate below 1 GHz. To design multi-antennas based on the T-strip loaded chassis, proper feeding techniques were analyzed to effectively excite one mode without disturbing the other. As a result, a dual-antenna system with high port-to-port isolation and low correlation was designed. The performance of the proposed dual-antennas was then evaluated in both free space and different user scenarios. The results indicate that the proposed design outperforms a reference dual-antenna design significantly as well as maintaining robustness against user influences. Practical factors (including the battery and glass of the mobile handset) and scenarios (indoor and outdoor scenario) are also investigated to show the value of the proposed antennas in real life.

The paper is organized as follows: In Section II, chassis modifications are studied in the framework of characteristic mode analysis. The potential of the modified chassis in providing uncorrelated antennas are demonstrated. Based on the T-strip loaded chassis, the feeding technique to effectively excite the T-mode and the single-antenna design are studied in Section III. Thereafter, design and simulations of orthogonal dual-antennas on the chassis are carried out in Section IV. MIMO performance analysis and different user scenarios are studied and compared with the reference antenna terminal in the same section. In Section V, a prototype of the proposed dual-antenna design was fabricated and the measured results are presented. Section VI gives the conclusions of the paper.

II. Chassis Modification

Characteristic mode analysis is an efficient method to gain physical insights into potential resonant and radiation characteristics of a structure by finding and examining its inherent modes. The characteristic modes are independent of the excitation, and only depend on the shape of the structure [22]. The analysis on these modes provides valuable information for antenna design.

An external electric field or voltage can induce a surface current on a conducting body, which can further generate a scattered field. With the boundary conditions and following the procedure in [23], characteristic mode is defined by the eigenvalues equation as

$$X(J_{s,n}) = \lambda_n R(J_{s,n}) \quad , \tag{1}$$

where X and R are the imaginary and real part of the impedance matrix, respectively. λ_n denotes the characteristic eigenvalues and $J_{s,n}$ is the eigenvector. To calculate the eigenvalues in Matlab, the linear equation (1) is transformed into a matrix equation using the method of moments (MoM) [24].

To begin with, the characteristic modes of a terminal planar chassis with a size of 120 mm × 60 mm were calculated, with its eigenvalues shown in Fig. 1. The modes in our work are numbered according to the order of occurrence of its resonant frequency. It is observed that only one mode (λ_1) can resonate at around 1 GHz, which is the flat dipole mode along the length of the chassis [13]. This mode can be easily excited by electric antennas (i.e., antennas whose near-field are dominated by electric field) implemented on the short edges of the chassis.

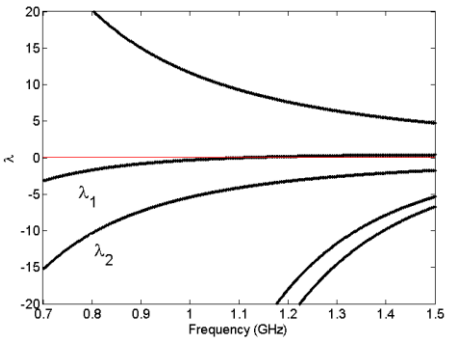

Fig. 1. Characteristic eigenvalues over frequency for a 120 mm × 60 mm chassis. The chassis material is Perfect Electric Conductor (PEC).

Due to the common use of electric antennas in terminals and the short chassis edges being convenient for antenna integration, severe mutual coupling among multi-antennas at frequencies around 1 GHz can often be attributed to the simultaneous excitation of the same dipole mode by the multi-antennas [13]. To obtain more characteristic modes that can resonate at around 1 GHz, the chassis structure should be modified. One example of chassis modification is to load the chassis with a bezel along its periphery [25], which can induce two inherently orthogonal modes at the same frequency band below 1 GHz. The drawback of the modification in [25] is the relatively narrow bezel resonance bandwidth.

In this section, we investigate a T-strip loaded chassis that provides a larger bandwidth potential. The geometries of the T-strip loaded chassis are shown in Fig. 2(a). Two metal strips along the length of the chassis are connected to the chassis through shorting pins at the center of each strip. The simple modification can be accommodated within typical dimensions of a smart phone, making it possible to implement in reality.

Using MoM, the eigenvalues of the T-strip loaded chassis are calculated and shown in Fig. 2(b). Three resonant modes are observed at frequencies below 1 GHz. Since Mode 2 (λ_2) has the narrowest bandwidth, it is not considered for the design of antennas. Mode 1 corresponds to the T-strip mode, whereas Mode 3 is the chassis' fundamental dipole mode.

To show the contribution of each mode in an explicit way, the modal significance [13] of these modes, as defined by

$$\mathrm{MS} = \left| \frac{1}{1 + j\lambda_n} \right|, \tag{2}$$

is plotted in Fig. 2(c). If we consider a modal significance criterion of 0.5, both Modes 1 and 3 have the potential to cover the bandwidth of 850-950 MHz, with Mode 3 having an even larger bandwidth. Therefore, once properly excited, Modes 1 and 3 can be used to achieve uncorrelated multi-antennas with a relatively large fractional bandwidth of around 10%.

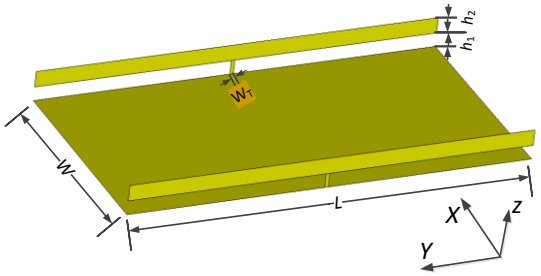

(a)

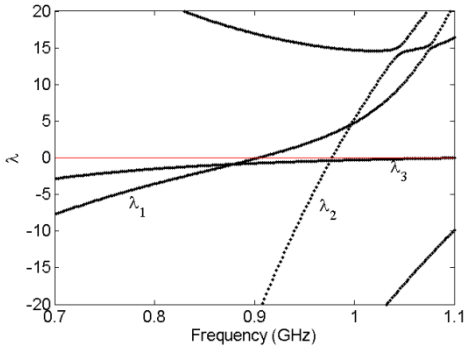

(b)

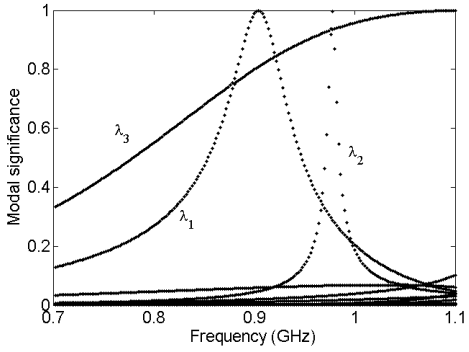

(c)

Fig. 2. (a) Geometries of the T-strip loaded chassis. The dimensions are: L = 120 mm, W = 60 mm, W_T = 0.5 mm, h_1= h_2=4 mm. (b) Eigenvalues of the T-strip loaded chassis. (c) Modal significance of the T-strip loaded chassis.

The total current on the surface of a conducting body can be expressed by the eigenvectors as [13]

$$J_s = \sum_n \frac{V_n^{ex} J_{s,n}}{1 + j\lambda_n}. \tag{3}$$

From the equation, it is seen that there are two factors determining the contribution of a certain mode to the total current distribution, i.e., the external excitation V_n^{ex} and the modal significance. Thus, the feeding method and position are also important for antenna operation. The feeding techniques for these two modes will be studied in Section III.

The normalized current distributions of the T-mode and the dipole mode (D-mode) at 900 MHz are presented in Fig. 3. As expected, the D-mode shows relatively strong currents all over the chassis, particularly along the longer edges of the chassis (i.e., like a flat dipole). The currents of the T-mode, on the contrary, are largely focused on the two metal strips, which exhibit the characteristic current of a top loaded dipole along the width (*x* axis) of the chassis [26].

Figure 4 shows the characteristic electric far-field patterns of the two modes. For the T-mode, the patterns on both *x*-*y* and *x*-*z* planes show a 'figure-eight' characteristic, and it is omnidirectional on the *y*-*z* plane. The patterns are consistent to those of an electric dipole along *x* axis, which further confirms the observation from the current distributions in Fig. 3(a). The patterns of the D-mode, on the other hand, exhibit a dipole placed along *y* axis. Though the magnitudes of the patterns of the two modes have some overlaps on the *x*-*z* and *y*-*z* planes, the polarizations of the two modes are different, with the main polarization of the D-mode along *y* axis and that of the T-mode along *x* axis. Hence, the radiation patterns remain uncorrelated.

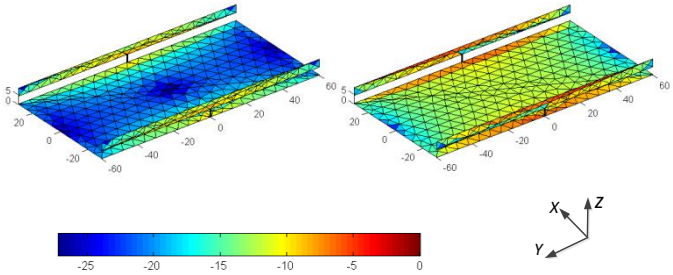

(a) T-mode (b) D-mode

Fig. 3. Normalized characteristic currents of both modes at 900 MHz.

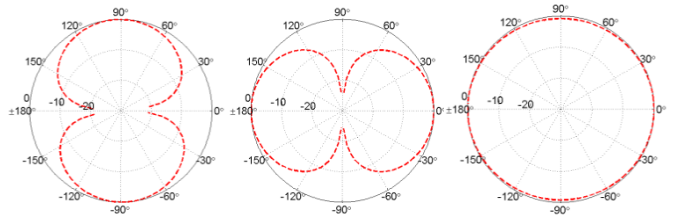

(a) T-Mode, *x*-*y* plane (b) T-Mode, *x*-*z* plane (c) T-Mode, *y*-*z* plane

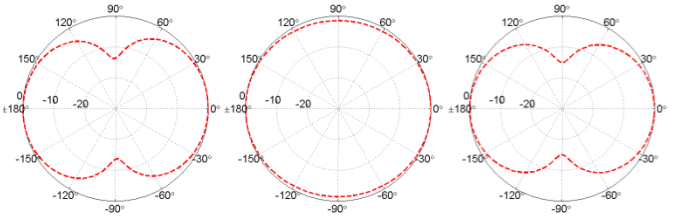

(d) D-Mode *x*-*y* plane (d) D-Mode, *x*-*z* plane (f) D-Mode, *y*-*z* plane

Fig. 4. Characteristic electric field patterns of the T-mode (Mode 1) and dipole (D-) mode (Mode 3) at 900 MHz.

The width of the shorting pin (W_T) is critical to the resonant frequency of the T-mode and its bandwidth. When the shorting pin becomes wider, the resonant frequency increases, and the bandwidth becomes larger. Apart from W_T, the reduction of the

total height (h_1+h_2) of the T-strip increases the resonant frequency and decreases the bandwidth of the T-mode. It is noted that the individual heights of h_1 and h_2 do not significantly affect the performance of the T-mode, if the total height is kept constant. This provides the mobile phone designers more freedom to determine the structure of the casing. The performance of the D-mode is largely unaffected by the variation of the T-strip.

The reactive near-fields of the T-strip loaded chassis are analyzed in order to provide valuable information for antenna feedings in Section III. The normalized magnitude of the characteristic electric (E) and magnetic (H) fields on a plane 10mm above the chassis for both the T-mode and the D-mode are shown in Fig. 5. It is seen that the magnitudes of total magnetic fields of the two modes are similar with each other, whereas the magnitudes of the total electric fields differ significantly. The x, y, z components of the E and H fields were also studied, though it is not shown here for the sake of conciseness. The E fields of both modes are dominated by the E_z component. For the H field, H_x plays an important role for the T-mode, whereas H_y is dominant for the D-mode. As expected of orthogonal modes, the reactive near fields of the two modes show good orthogonality.

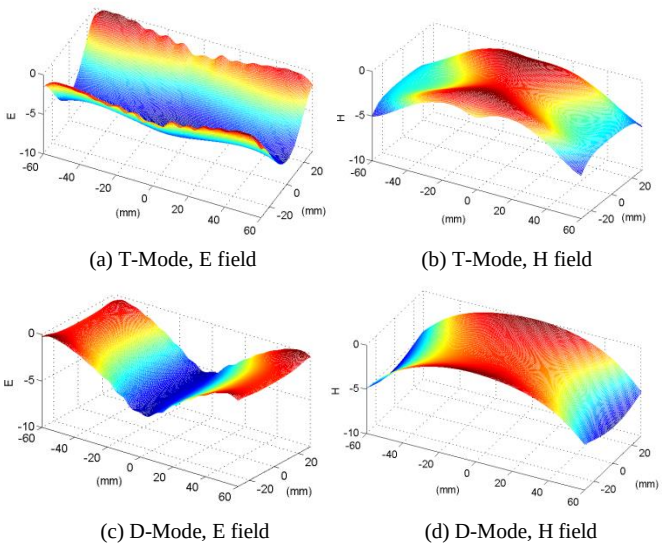

(a) T-Mode, E field (b) T-Mode, H field

(c) D-Mode, E field (d) D-Mode, H field

Fig. 5. Normalized magnitude of electric and magnetic fields of both modes at 900 MHz.

III. Single Antenna Design Based on T-mode

In order to excite a certain mode of the chassis, the biggest challenge is to find the effective feeding structure and feeding locations. For the fundamental D-mode of the chassis, which is well known and frequently utilized for mobile antennas, there exist a number of excitation methods, such as placing a PIFA or a monopole on a short edge of the chassis [27], [28]. Consequently, in this section, we focus on the antenna design for the newly introduced T-mode of the chassis. Full-wave antenna simulations were carried out in the frequency domain using CST Microwave Studio.

The main strategy for feeding the T-mode is to obtain good impedance matching and large bandwidth for the T-mode without exciting the D-mode. One way to determine the optimal feeding location is by looking into the locations of the minimum and maximum characteristic currents for each driven mode. According to this approach, we first applied a direct feeding at one of the shorting pins to excite the T-mode, since the current is strong along the shorting pins. A resonance was successfully created in the simulation; however, the impedance matching was poor due to the small radiation resistance of around 10 Ω.

As an alternative feeding method, the reactive near-field behaviors of the characteristic mode were studied, since they give insights into where the coupled energy can be maximized for a given mode, while reducing the probability of coupling to other modes. The difference in the electric fields between the T-mode (Fig. 5(a)) and the D-mode (Fig. 5(c)) enables the excitation of one mode without significantly affecting the other mode. If capacitive coupling, which is used to couple to the characteristic electric field [29], is created at the center of one of the chassis' longer edges, then the T-mode is strongly excited. On the other hand, the D-mode is only weakly excited by the capacitive coupling because its characteristic E field is very small at this feeding location. Similarly, if the capacitive coupling is located at the center of one shorter edge of the chassis, only the D-mode is strongly excited.

Based on the above analysis, the T-strip antenna is designed and its geometries are shown in Fig. 6(a). A small narrow plate parallel to the chassis is used to create capacitive coupling close to the center of one longer chassis edge, in order to excite the T-mode. The plate is connected to one of the T strips, and it is fed by a vertical strip with a lateral (edge-to-edge) distance of 2mm from the shorting pin of the T strip. The width of the shorting pin is 0.5 mm. A discrete port (indicated by the red arrow in Fig. 6(a)) is used in the simulation to feed the antenna, and a lumped capacitor of 1.5 pF is applied in series at the port to improve the impedance matching. For ease of fabrication, a FR4 substrate, with a permittivity of 4.3, a loss tangent of 0.014 and a thickness of 0.8 mm, is utilized under the ground plane. It has been verified in the simulation that the substrate does not significantly affect the resonant frequency and the bandwidth of the T-strip antenna. The magnitude of the reflection coefficients for the T-strip antenna (blue curve) is shown in Fig. 7. It is observed that the 6 dB impedance bandwidth of the antenna is from 868 MHz to 979 MHz, which covers the whole LTE Band 8.

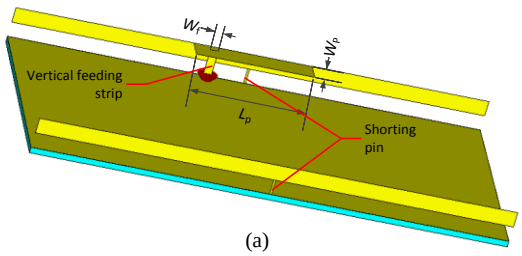

(a)

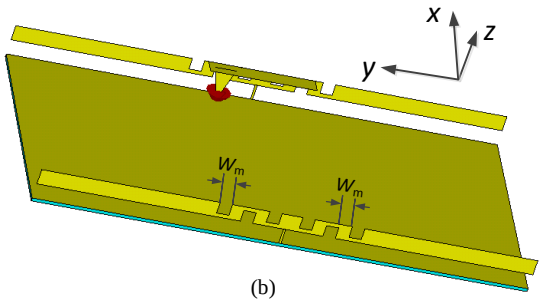

(b)

Fig. 6. Geometries of (a) T-strip antenna without meander line, and (b) T-strip antenna with meander line. The dimensions are: L_P = 30 mm, W_P = 6 mm, W_f = 2 mm, W_m = 3 mm. Other dimensions are identical to those in Fig. 2.

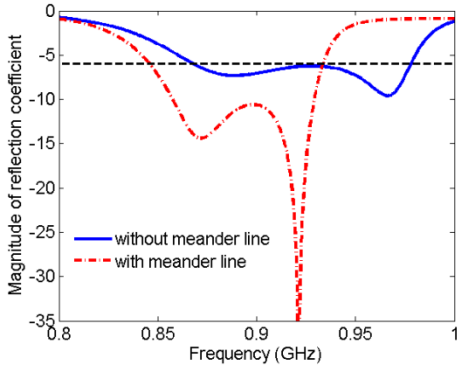

Fig. 7. Magnitude of the reflection coefficient for the T-strip antenna with and without meander line.

To show the possibility of the antenna to resonate at lower frequency bands, modifications are made to the T strips, as presented in Fig. 6(b). In order to increase the electrical length of the T-mode, square shapes with a width of 3 mm are etched symmetrically about the shorting pin on each of the two T-strips to form meandered structures. The distance between the adjacent squares is also 3 mm. Since the characteristic currents of the T-mode are strong in vicinity of the center of the strips (see Fig. 3(a)), each strip structure is mainly meandered around the center to maximize the effectiveness of lowering the resonant frequency. The vertical feeding strip is tapered (i.e., width of 5 mm at the top and 1 mm at the bottom) due to its better impedance matching behavior [30]. For comparison, the magnitude of the reflection coefficients of the meandered T-strip antenna (red curve) is also shown in Fig. 7. The center frequency of the antenna is reduced by 30 MHz after it is meandered. As a trade-off, the bandwidth of the T-strip antenna is reduced from 111 MHz to 90 MHz.

IV. Orthogonal Dual-Antenna System

A. Antenna Structures

In this section, a practical MIMO terminal antenna system, consisting of a coupled fed monopole antenna [31] and a T-strip antenna, is proposed. Monopole antennas, which are commonly used in mobile phones, can effectively excite the D-mode of the chassis to obtain a large bandwidth [13]. The geometries of the antenna system are presented in Fig. 8. The monopole, with a volume of 40 × 7 × 3 mm^3, is comprised of three parts: the feeding strip, the coupling strip and the main radiator. It is mounted onto a hollow carrier, which is hidden in the figure for a better view. The carrier has a thickness of 1 mm, a permittivity of 2.7 and a loss tangent of 0.007. A lumped capacitor of 2 pF is used in series at the port of monopole to better match the antenna. In order to keep the surface area of the mobile phone to 120 mm × 60 mm, the chassis ground plane was shortened to 113 mm to provide space for the monopole antenna. For ease of fabrication, the T-strips were printed on the same FR4 substrate as in Section III. Due to the higher permittivity (4.3) of FR4 as compared with air, the length of the T-strip is reduced to maintain the same resonant frequency. If a lower resonant frequency is desired, the strip length can be increased. Alternatively, the strip may be meandered, as suggested in Section III.

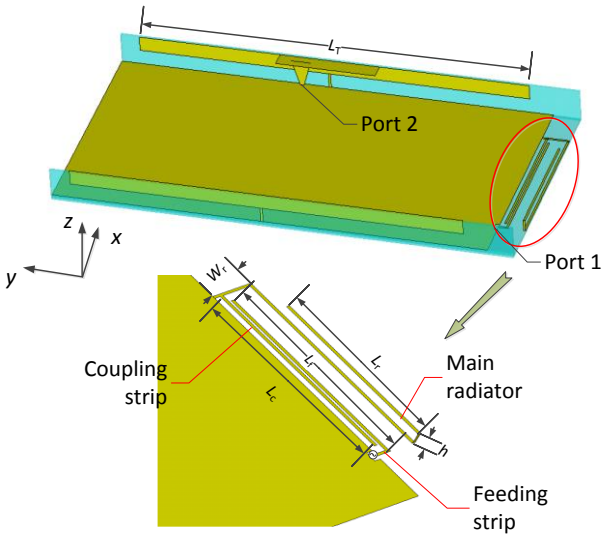

Fig. 8. Geometries of the proposed dual-antenna system. The dimensions are: L_T = 102 mm, W_t = 4 mm, L_r = 32 mm, L_c = 37.5 mm, L_f = 37.5 mm, h = 3 mm.

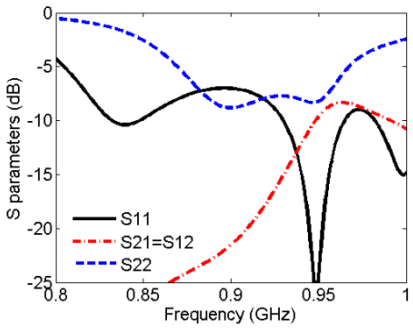

Fig. 9. S parameters of the proposed dual-antenna system.

The simulated magnitudes of the scattering (S) parameters for the dual-antenna terminal are shown in Fig. 9. The T-strip antenna operates within the bandwidth of 875-964 MHz, and the monopole covers a larger bandwidth from 809 MHz to 1 GHz. The antenna isolation is above 8.5 dB within the common band of both antennas. In particular, for frequencies below 935 MHz, the isolation is above 15 dB. This is owing to the orthogonality of the two modes, i.e., the D-mode and the T-mode, created by the two antennas. However, the isolation becomes worse as the frequency increases towards 964 MHz. This can be explained by the modal significance in Fig. 2(c), where the D-mode provides the dominant contribution at frequencies above 950 MHz. According to (3), since the total

current distribution depends on both the excitation and the significance of the relevant modes, though the feeding of the T-strip antenna is at a suitable location to efficiently induce the T-mode at the center frequency of around 900 MHz, it is difficult to guarantee that it does not affect the D-mode over the whole operating band. At frequencies close to 960 MHz, the D-mode also contributes to the total current due to its higher modal significance above 950 MHz, as well as the feeding location not being optimized for exciting only the T-mode at these frequencies. As a result, the orthogonality between the ports is deteriorated, which is verified by the higher correlation at 0.96 GHz in Fig. 14 (a). The deterioration of orthogonality leads to worse isolation than that which was achieved at lower frequencies. To improve the isolation between the antennas, we can either change the feeding technique (including coupling methods and positions) or the T-strip structure by analyzing the characteristic fields over a larger bandwidth. Moreover, with minor changes in the feeding and the T-strip, the proposed antenna system can also be designed to operate in multiple bands with good isolation. However, since this paper focuses on the design of uncorrelated MIMO antennas at frequencies below 1 GHz, no explicit effort was made to optimize the multi-band performance.

B. MIMO Performance

MIMO channel capacity is one of the most popular metrics for evaluating the performance of multiple antenna systems. In this paper, the capacity is calculated for 2×2 antenna setup at different frequencies under the waterfilling (WF) condition [32] for a reference signal-to-noise ratio (SNR) of 20 dB. The WF procedure is performed over the antenna elements at each frequency. The Kronecker model [33] and uniform 3D angular power spectrum (APS) are assumed. Kronecker model is used due to its simplicity and its ability to incorporate non-ideal multi-antenna effects of correlation, power (efficiency) loss and efficiency difference into the ideal Rayleigh identical and independently distributed (IID) channel. The model has also been experimentally verified to be valid for 2 × 2 MIMO systems [34]. In the simulation, it is assumed that there is no correlation between the base station transmit antennas, whereas the (terminal) receive antennas are correlated according to their patterns and the uniform 3D APS. The capacity is averaged over 10,000 IID Rayleigh realizations [32] at each frequency. The channels are normalized with respect to the IID Rayleigh case, which means that the correlation, total antenna efficiency and efficiency imbalance are taken into account in the capacity evaluation.

The simulated total efficiencies of the proposed antennas are presented in Fig. 19. Within LTE Band 8, the efficiencies of the monopole antenna and the T-strip antenna are around -1.5 dB and -2 dB, respectively. The monopole antenna also radiates efficiently at LTE Band 5, at which the efficiency of the T-strip antenna is low due to poor impedance matching. The ECC of the proposed dual-antenna terminal in free space is shown in Fig. 14(a).

For comparison, the dual-antenna terminal proposed in [12] was chosen as the reference antenna. The reference design was also simulated in the frequency domain using CST Microwave Studio. To better compare the two antenna designs, the reference antenna was marginally re-tuned to be resonant at the same frequency band as the proposed antennas. The S parameters of the retuned reference antenna system are presented in Fig. 10, together with its structure. It can be seen that the reference antenna terminal has a large bandwidth, with a minimum isolation of around 9 dB. The total efficiencies of both antennas in free space are around -2.3 dB, as reported in [12]. The ECCs calculated from the far field patterns are around 0.5 over the frequency band of 824-960 MHz, which leads to some degradation in the MIMO performance.

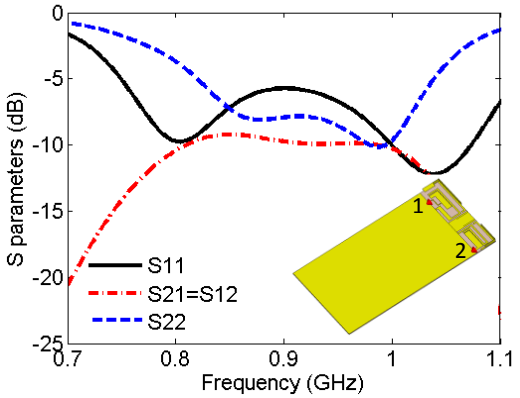

Fig. 10. S parameters of the reference antenna system, with its structure shown in the subset.

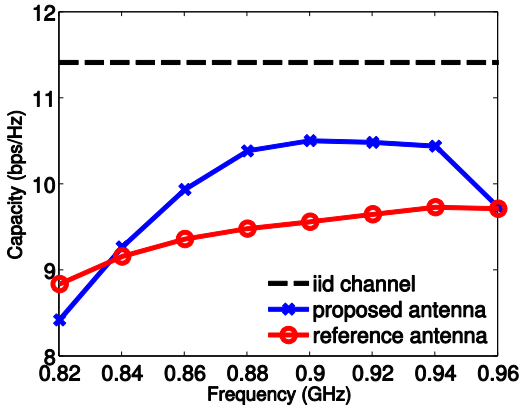

Fig. 11. Channel capacities for three different cases.

The channel capacities for three cases are presented in Fig. 11, i.e., the IID Rayleigh channel, the proposed dual-antenna terminal, and the reference dual-antenna terminal. The IID case corresponds to the ideal situation of 100% total antenna efficiencies and zero correlation between the antennas. Within LTE Band 8, for which the T-strip antenna is designed for, the average channel capacity over the band is around 1 bps/Hz higher than that of the reference antenna terminal. Even at LTE Band 5, the channel capacity of the proposed antenna is generally higher even though the T-strip antenna is not well matched. The only exception is for frequencies below 840 MHz, since then the reflection coefficient of the T-strip antenna is so high that it hardly radiates any power. Considering that MIMO schemes in LTE are only used in the downlink, which corresponds to 869-894 MHz for LTE Band 5, the proposed antenna terminal still outperforms the reference antenna terminal. Compared with the IID channel, the drop of the channel capacity for the proposed antenna terminal is mainly

due to its limited antenna efficiencies, since the ECC is quite low (below 0.07) over the band of interest. It is noted that the substrate used for the T-strips is FR4 with relatively high loss tangent. If materials with lower loss tangents (e.g., 0.002) are used for the antenna casing, the total efficiency of the T-strip antenna can be increased by up to 10%, leading to a higher channel capacity of the proposed antenna terminal.

The MIMO performances in more practical propagation scenarios (i.e., indoor and outdoor scenarios) were also studied in postprocessing using CST. A uniform distribution was assumed for the azimuth plane [35], since the direct path from the base station to the mobile terminal is usually blocked by some obstacles, and local scattering objects are often present around the terminal. For the elevation plane, two common distributions, i.e. Gaussian and Laplacian distributions, were considered. Correlation and mean effective gain (MEG) [35], were used to characterize the MIMO performance. The results show that, for both the proposed antenna system and the reference antenna system, the correlation between the antenna elements do not vary significantly between the ideal uniform case and the practical scenarios. On the other hand, the MEG varies significantly with the considered scenario, with the proposed antenna giving higher MEG but with larger fluctuations than the reference antenna at frequencies between 860-960 MHz. In general, MIMO performance has been found to deteriorate with non-uniform APS (i.e., practical scenarios). However, the ideal and the practical cases give similar relative performance trends between the proposed antenna and the reference antenna, and the proposed antenna outperforms the reference antenna within the designed bands.

C. User Effects

This subsection explores the effects of hand loading on the performance of the proposed dual-antenna terminal. Two scenarios, i.e., one-hand (OH) data mode and two-hand (TH) data mode, are investigated. Figure 12 illustrates the position of the hands with respect to the terminal for the two scenarios. The two scenarios are chosen because they are representatives of common user cases, where users either browse their devices or play games. The exact grip positions of the OH and TH data modes closely follow the studies in [36] and [37], respectively.

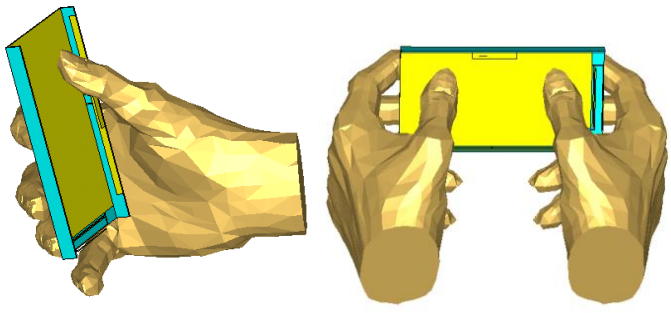

(a) (b)

Fig. 12. Positions of hand(s) with respect to the terminal antennas for (a) one-hand (OH) data mode and (b) two-hand (TH) data mode.

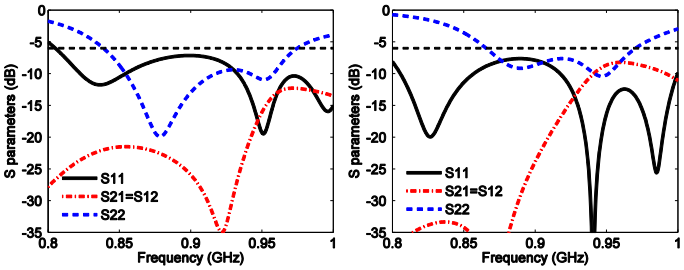

(a) (b)

Fig. 13. Magnitudes of S parameters for (a) OH data mode and (b) TH data mode.

Figure 13 presents the S parameters for the OH and TH cases. In general, the proposed antenna system fully covers the LTE Band 8 for both scenarios. In addition, the monopole (Port 1) also covers LTE Band 5 in both scenarios. In the OH scenario, the palm is closer to the T-strip antenna, whereas in the TH case the palm is closer to the monopole antenna. Thus, compared with the free space scenario, it can be expected that the resonance of the T-strip antenna is more influenced in the OH case, and that of the coupled monopole is more affected by the TH case [38], as has been verified in Fig. 13. In general, the port isolation between the antennas becomes higher as compared with the free space scenario, owing to the high absorption loss in the hand tissue. However, the isolation at around 960 MHz is not noticeably improved in the TH scenario. In fact, higher correlation is observed in this frequency region as shown in Fig. 14(a). This is caused by significant reshaping of the antenna patterns by the presence of the hands, which reduces their orthogonality. In genernal, the ECC in the proposed antenna terminal is very low for all the scenarios. The rule of thumb that the ECC should be no higher than 0.5 for good MIMO performance [39] is satisfied even at 960 MHz.

The total efficiencies of the dual-antennas in different scenarios are shown in Fig. 14(b). Compared with the free space scenario, the efficiencies of both the monopole and the T-strip antenna in the OH scenario drop by 2 dB at LTE Band 8. However, within 820-850 MHz, the efficiency of the T-strip antenna in the OH scenario even outperforms that in free space, due to its better impedance matching. In the TH scenario, the efficiency of the T-strip antenna is similar as that for the OH case, whereas the efficiency of the monopole is decreased by another 1 dB. Since the impedance matching is good for all the scenarios, the drop of efficiencies is mainly due to the absorption loss in the hand tissues. The channel capacities of the proposed dual-antenna system with user effects are shown in Fig. 15, together with those of the reference antenna system. The ground planes for the two antenna systems were aligned in the same positions, with respective to the hand(s). For the OH case, the antenna elements in the reference terminal were placed at the bottom, similar to the placement of the monopole in the proposed terminal. It is observed that the proposed design significantly outperforms the reference terminal (i.e., by up to 1.5 bps/Hz at 20dB SNR) in the OH user scenario. For the TH scenario, the proposed antenna has a lower capacity at 0.82-0.84 GHz and 0.94-0.96 GHz due to the relatively lower efficiency of the T-strip antenna. However, the averaged

capacities (over LTE Band 8) for the TH case are similar for the two dual-antenna systems.

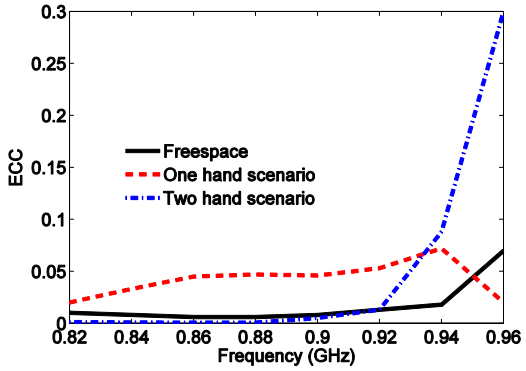

(a)

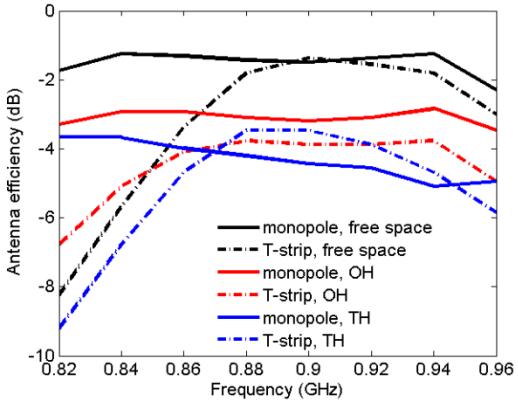

(b)

Fig. 14. (a) ECC for three different scenarios; (b) Total antenna efficiencies for three different scenarios.

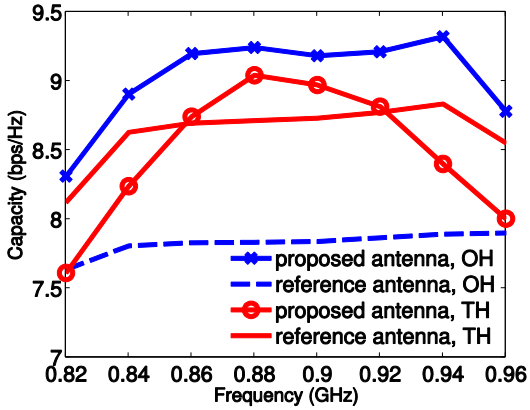

Fig. 15. Channel capacities for different user scenarios.

To investigate the proposed antenna practically, two realistic components, i.e., the battery and the casing, were added to the proposed antenna. In the simulation, the battery was modeled as a copper block with the dimensions of 100 × 50 × 5 mm^3 and a conductivity of 5.8×10^7 S/m. To represent the casing, a glass material with a permittivity of 3.5 and a loss tangent of 0.02 was added around the ground plane, similar as the casing of Apple Iphone 4S. We use the loss tangent of 0.02 and a thickness of 1 mm to represent the worst case, since actual casings (including normal plastic ones) are usually less lossy and thinner. From the simulation, it was found that the battery does not have much influence on the operation of the antennas. On the other hand, the glass can lower the resonant frequency and the total efficiencies of the antennas, especially for the T-strip antenna. With the addition of both the glass and the battery, the operating band of the monopole was not significantly affected, whereas the T-strip antenna now operates at a lower frequency and with a narrower bandwidth. However, by reshaping the T-strip, the resonance can be retuned to the desired frequency. The total antenna efficiencies averaged over 0.82-0.96 GHz were also compared. With the glass and the battery, the efficiencies of monopole and the T-strip antennas were reduced by 0.32 dB and 0.85 dB, respectively. The efficiency drop of the T-strip antenna mainly occurred near the upper band edge, due to its shift in resonance, which can be somewhat compensated with retuning.

V. Experiments and Discussions

The proposed antenna system was fabricated and shown in Fig. 16. Six L-shaped supporting frames are used to connect the substrate of the T-strip antenna with the flat chassis. The influence of the supporting frames was studied in the simulation. It was determined that they decrease the resonant frequency of the T-strip antenna by 2 MHz and deteriorate the matching by 0.5 dB. Two capacitors as in the simulation, i.e., 1.5 pF for the T-strip antenna and 2 pF for the monopole antenna, were used in the prototype. The SMA feeds of the two antennas are placed at a shorter edge of the chassis, since the longer edges of the chassis are occupied by the T-strips. In practice, it has been found that placing the SMA feed along the longer edges reduces the influence of cable in the measurement results for both the single-antenna [40] and multi-antenna cases [41]. However, external cable feed is not required in real mobile antenna integration.

The S parameters were measured with a vector network analyzer and shown in Fig. 17. The measured results show that both antennas cover LTE Band 8 with an isolation of above 10 dB.

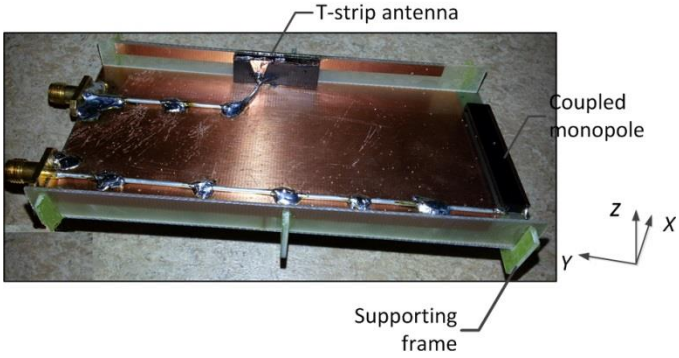

Fig. 16. Prototype of the dual-antenna mobile terminal system, consisting of the coupled monopole and the T-strip antenna.

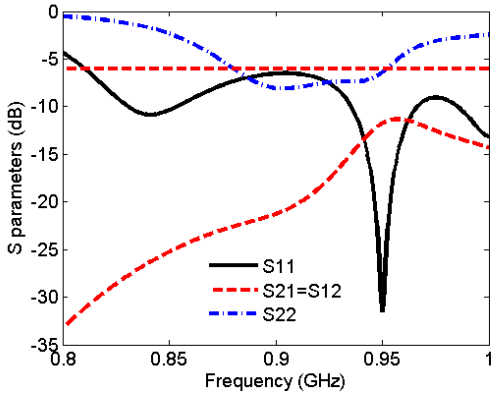

Fig. 17. Measured S parameters of the dual-antenna mobile terminal system.

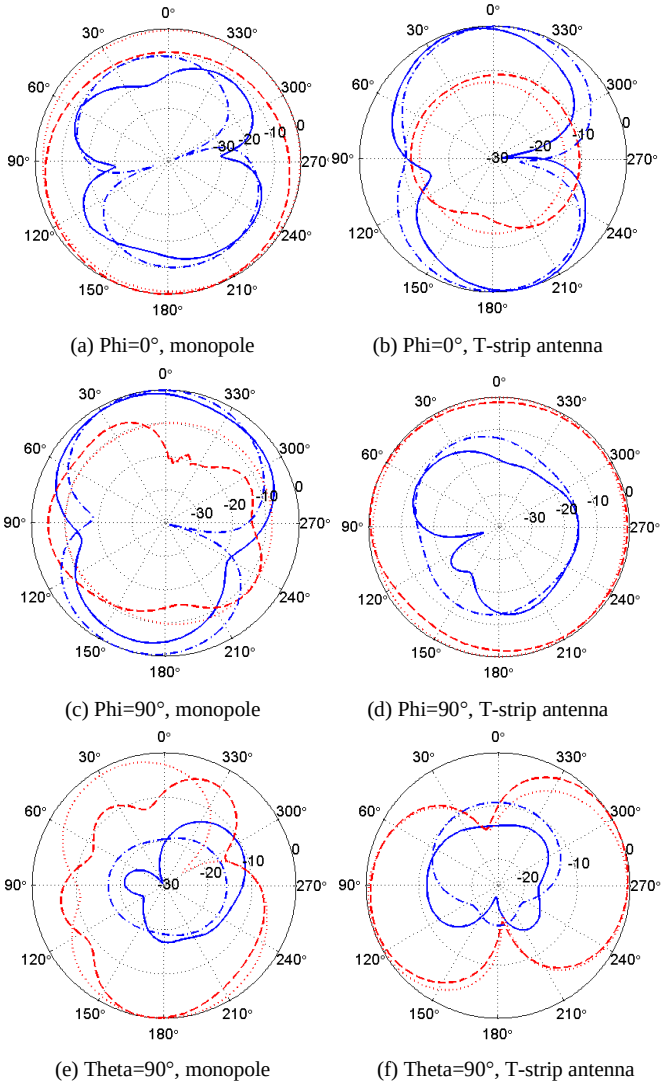

(a) Phi=0°, monopole (b) Phi=0°, T-strip antenna

(c) Phi=90°, monopole (d) Phi=90°, T-strip antenna

(e) Theta=90°, monopole (f) Theta=90°, T-strip antenna

Fig. 18. Simulated and measured antenna patterns for the co-located antenna system: (--) measured *E*(Theta), (– –) simulated *E*(Theta), (– -)measured *E*(Phi), (—) simulated *E*(Phi).

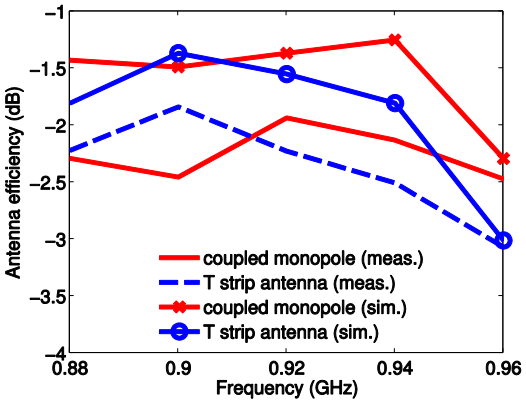

Fig. 19. Simulated and Measured total efficiencies of the proposed dual-antenna system.

The far-field patterns and total efficiencies of the antenna were measured in a Satimo Stargate-64 antenna measurement facility. In general, the measured patterns agree well with the simulated ones, as can be seen in Fig. 18. At Phi = 90° plane, i.e., *y*-*z* plane, slight difference occurs around Theta = 90°, which corresponds to the location of the SMA connectors and the feed cables. The difference in the plane of Theta = 90° is due to the same reason. From the measured radiation patterns, it is clear that both pattern and polarization diversities are achieved in the proposed antenna. The ECCs calculated from the measured patterns are 0.1, 0.12 and 0.16 at 880MHz, 920 MHz and 960 MHz, respectively, which are higher than those in the simulation. This is mainly attributed to the SMA connectors and the cable influence.

The simulated and measured efficiencies for the coupled monopole and the T-strip antenna at LTE Band 8 are presented in Fig. 19. The measured efficiencies are around 0.5 dB lower than the simulated ones. Simulations were carried out to study the possible factors that led to the discrepancy. It was found that on average, the supporting frames used in the measurement can incur a loss of 0.1 dB. The deterioration in impedance matching can account for additional losses of 0.15 dB and 0.24 dB for the monopole and T-strip antennas, respectively. The non-ideal capacitors, assuming a series loss resistance of 2 Ω, can induce losses of 0.08 dB and 0.05 dB for the monopole and T-strip antennas, respectively.

VI. Conclusion

In this work, a novel and practical approach to designing an uncorrelated dual-antenna mobile terminal at frequencies below 1 GHz is proposed. Through manipulating the chassis in a reasonable manner, it is possible to excite previously non-excitable orthogonal modes at frequency bands below 1 GHz. In order to induce these non-existent modes in a planar mobile chassis, T-strips were added to load the chassis and allow for excitation of two separate modes. These inherently orthogonal modes, i.e., the D-mode and T-mode, were designed to resonate at the same frequency band. Through utilizing the characteristic near fields, it was possible to determine feeding techniques to excite each antenna mode without coupling to the

other.

The proposed antenna system was studied in three different scenarios: free space, OH case and TH case. The ECC between the two antennas in free space is below 0.1 over the operating band. The results also show that the S parameters and the ECCs were only marginally influenced by the hands, whereas the efficiencies were decreased due to the absorption loss of the hand tissue. Moreover, the proposed antenna was compared with a state-of-the-art reference antenna system, and it was found that the capacity of the proposed design is higher than that of the reference design by up to 1 bps/Hz in free space and 1.5 bps/Hz in the OH scenario, at a reference SNR of 20dB. The potential of the proposed antenna to operate in multiple bands are also shown in the paper. Besides, practical considerations, such as the integration of battery and glass display in the mobile handset and different APS in real environments, are taken into account to further demonstrate the robustness of the proposed antenna.

It is noted that besides the T-strip structure, the design concept of enabling multiple orthogonal resonant modes below 1 GHz by modifying the chassis structure can be applied to design other uncorrelated antenna structures that can be optimized for improved performances. As future work, we will apply the characteristic mode analysis in a more systematic manner to design multi-band antennas and their feeds. We will also employ the design concept in this paper to achieve uncorrelated multi-antennas with more than two antenna elements.

REFERENCES

[1] M. A. Jensen and J. W. Wallace, "A review of antennas and propagation for MIMO wireless communications," *IEEE Trans. Antennas Propag.*, vol. 52, pp. 2810-2824, Nov 2004.

[2] B. K. Lau, "Multiple antenna terminals," in *MIMO: From Theory to Implementation*, C. Oestges, A. Sibillea, and A. Zanella, Eds., San Diego: Academic Press, 2011, pp. 267-298.

[3] B. K. Lau, J. B. Andersen, G. Kristensson, and A. F. Molish, "Impact of matching network on bandwidth of compact antenna arrays," *IEEE Trans. Antennas Propag.*, vol. 54, pp. 3225-3238, Nov 2006.

[4] H. Li, J. Xiong, and S. He, "A compact planar MIMO antenna system of four elements with similar radiation characteristics and isolation structure," *IEEE Antennas Wireless Propag. Lett.*, vol. 8, pp. 1107-1110, 2009.

[5] H. Li, J. Xiong, Z. Ying, and S. He, "High isolation compact four-port MIMO antenna systems with built-in filters as isolation structure," in *Proc. 4th Europ. Conf. Antennas Propag. (EUCAP)*, Barcelona, Spain, Apr. 12-16, 2010.

[6] A. Diallo, C. Luxey, P. Le Thuc, R. Staraj, and G. Kossiavas, "Enhanced two-antenna structures for universal mobile telecommunications system diversity terminals," *IET Microw. Antennas Propag.*, vol. 2, pp. 93-101, Feb 2008.

[7] B. K. Lau and J. B. Andersen, "Simple and efficient decoupling of compact arrays with parasitic scatterers," *IEEE Trans. Antennas Propag.*, vol. 60, pp. 464-472, Feb 2012.

[8] D. Manteuffel and R. Martens, "Multiple antenna integration in small terminals," in *Proc. Int. Symp. Antennas Propag. (ISAP'2012)*, Nagoya, Japan, Oct.29-Nov.2, 2012.

[9] R. A. Bhatti, S. Yi, and S. O. Park, "Compact antenna array with port decoupling for LTE-standardized mobile phones," *IEEE Antennas Wireless Propag. Lett.*, vol. 8, pp. 1430-1433, 2009.

[10] G. Park, M. Kim, T. Yang, J. Byun, and A. S. Kim, "The compact quad-band mobile handset antenna for the LTE700 MIMO application," in *Proc. IEEE Int. Symp. Antenna Propag. (APSURSI)*, South Carolina, US, 2009.

[11] M. S. Han and J. Choi, "Multiband MIMO antenna with a band stop filter for high isolation characteristics," in *Proc. IEEE Int. Symp. Antenna Propag. (APSURSI)*, South Carolina, US, 2009.

[12] K. L. Wong, T. W. Kang, and M. F. Tu, "Internal mobile phone antenna array for LTE/WWAN and LTE MIMO operations," *Microw Opt Techn Let*, vol. 53, pp. 1569-1573, Jul 2011.

[13] H. Li, Y. Tan, B. K. Lau, Z. Ying, and S. He, "Characteristic mode based tradeoff analysis of antenna-chassis interactions for multiple antenna terminals," *IEEE Trans. Antennas Propag.*, vol. 60, pp. 490-502, Feb. 2012.

[14] H. Li, B. K. Lau, Z. Ying, and S. He, "Decoupling of multiple antennas in terminals with chassis excitation using polarization diversity, angle diversity and current control," *IEEE Trans. Antennas Propag.*, vol. 60, pp. 5947-5957, Dec 2012.

[15] H. Li, B. K. Lau, Y. Tan, S. He, and Z. Ying, "Impact of current localization on the performance of compact MIMO antennas," in *Proc. 5th Europ. Conf. Antennas Propag. (EuCAP'2011)*, Rome, Italy, Apr. 11-15, 2011, pp. 2423-2426.

[16] C. T. Lee and K. L. Wong, "Internal WWAN clamshell mobile phone antenna using a current trap for reduced ground plane effects," *IEEE Trans. Antennas Propag.*, vol. 57, pp. 3303-3308, Oct 2009.

[17] J. Holopainen, J. Ilvonen, O. Kivekas, R. Valkonen, C. Icheln, and P. Vainikainen, "Near-field control of handset antennas based on inverted-top wavetraps: focus on hearing-aid compatibility," *IEEE Antennas Wireless Propag. Lett.*, vol. 8, pp. 592-595, 2009.

[18] P. Lindberg and E. Ojefors, "A bandwidth enhancement technique for mobile handset antennas using wavetraps," *IEEE Trans. Antennas Propag.*, vol. 54, pp. 2226-2233, Aug. 2006.

[19] M. Sonkki, E. A. Daviu, M. F. Bataller, and E. Salonen, "Performance comparison of a symmetrical folded dipole antenna for mobile terminals and its metal bezel extension," in *Proc. 5th Europ. Conf, Antennas Propag. (EuCAP'2011),* , Italy, Rome, Apr. 11-15, 2011, pp. 1913-1916.

[20] Q. Guo, R. Mittra, F. Lei, J. Ju, and J. Byun, "Interaction between internal and external antenna of mobile phone and hand effect," *IEEE Trans. Antennas Propag.*, vol. 61, pp. 862-870, Feb 2013.

[21] M. Pascolini, R. J. Hill, J. Zavala, N. Jin, Q. Li, R. W. Schlub, and R. Caballero, "Bezel gap antennas," U. S. Patent 8270914, Sep 18, 2012.

[22] M. Cabedo-Fabres, E. Antonino-Daviu, A. Valero-Nogueira, and M. F. Bataller, "The theory of characteristic modes revisited: A contribution to the design of antennas for modern applications," *IEEE Antennas Propag. Mag*, vol. 49, pp. 52-68, Oct 2007.

[23] R. F. Harrington and J. R. Mautz, "Computation of characteristic modes for conducting bodies," *IEEE Trans. Antennas Propag.*, vol. AP19, pp. 629-639, Sep. 1971.

[24] S. N. Makarov, *Antenna and EM modeling with Matlab*, New York: Wiley-Interscience, 2002.

[25] H. Li, Z. Mier, and B. K. Lau, "Generating multiple characteristic modes below 1GHz in small terminals for MIMO antenna design," in *Proc. IEEE Int. Symp. Antenna Propag. (APSURSI'2013)*, Orlando, FL, USA, Jul. 7-13, 2013.

[26] A. W. Rudge, A. David Olver, K. Milne, and P. Knight, *The Handbook of Antenna Design*, vol. 2, London: P. Peregrinus, 1983.

[27] P. Vainikainen, J. Ollikainen, O. Kivekas, and K. Kelander, "Resonator-based analysis of the combination of mobile handset antenna and chassis," *IEEE Trans. Antennas Propag.*, vol. 50, pp. 1433-1444, Oct 2002.

[28] S. R. Best, "The significance of ground-plane size and antenna location in establishing the performance of ground-plane-dependent antennas," *IEEE Antennas Propag. Mag*, vol. 51, pp. 29-43, Dec. 2009.

[29] R. Martens, E. Safin, and D. Manteuffel, "Inductive and capacitive excitation of the characteristic modes of small teminals," in *Proc. LAPC*, UK, Nov., 2011.

[30] R. Valkonen, J. Ilvonen, C. Icheln, and P. Vainikainen, "Inherently non-resonant multi-band mobile terminal antenna," *Electron Lett*, vol. 49, pp. 11-12, Jan 3 2013.

[31] K. J. Kim, S. Lee, B. N. Kim, J. H. Jung, and Y. J. Yoon, "Small antenna with a coupling feed and parasitic elements for multiband mobile applications," *IEEE Antennas Wireless Propag. Lett.*, vol. 10, pp. 290-293, 2011.

[32] A. Paulraj, R. Nabar, and D. Gore, *Introduction to Space-time Wireless Communications*, Cambridge; New York: Cambridge University Press, 2003.

[33] J. P. Kermoal, L. Schumacher, K. I. Pedersen, P. E. Mogensen, and F. Frederiksen, "A stochastic MIMO radio channel model with

experimental validation," *IEEE J. Sel. Area Commun.*, vol. 20, pp. 1211-1226, Aug. 2002.

[34] K. Yu, M. Bengtsson, B. Ottersten, D. McNamara, P. Karlsson, and M. Beach, "Second order statistics of NLOS indoor MlMO channels based on 5.2 GHz measurements," in *Proc. IEEE Global Commun. Conf. (Globecom)*, San Antonio, TX, 2001, pp. 156-160.

[35] T. Taga, "Analysis for mean effective gain of mobile antennas in land mobile radio environments," *IEEE Trans. Veh. Technol.,* vol. 39, pp. 117-131, May 1990.

[36] V. Plicanic, I. Vasilev, R. Tian, and B. K. Lau, "Capacity maximisation of handheld MIMO terminal with adaptive matching in indoor environment," *Electron Lett*, vol. 47, pp. 900-901, Aug. 4, 2011.

[37] M. Pelosi, O. Franek, M. B. Knudsen, M. Christensen, and G. F. Pedersen, "A grip study for talk and data modes in mobile phones," *IEEE Trans. Antennas Propag.*, vol. 57, pp. 856-865, Apr. 2009.

[38] M. Pelosi, O. Franek, M. B. Knudsen, G. F. Pedersen, and J. B. Andersen, "Antenna proximity effects for talk and data modes in mobile phones," *IEEE Antennas Propag. Mag*, vol. 52, pp. 15-27, Jun 2010.

[39] R. G. Vaughan and J. B. Andersen, "Antenna diversity in mobile communications," *IEEE Trans. Veh. Technol.,* vol. 36, pp. 149-172, Nov 1987.

[40] X. Lu, Y. Liu, and H. Kim, "Analysis of cable effect in portable antennas," in *Proc. Progress In Electromagnetics Research (PIERS) Symp.*, Malaysia, March 27-30, 2012, pp. 1483-1486.

[41] V. Plicanic, B. K. Lau, A. Derneryd, and Z. N. Ying, "Actual diversity performance of a multiband diversity antenna with hand and head effects," *IEEE Trans. Antennas Propag.*, vol. 57, pp. 1547-1556, May 2009.